Journal of the Korean Ceramic Society
Vol. 53, No. 4, pp. 393~399, 2016.

http://dx.doi.org/10.4191/kcers.2016.53.4.393

Minimization of Recombination Losses in 3D Nanostructured TiO_2 Coated with Few Layered g-C_3N_4 for Extended Photo-response

Suhee Kang, Rajendra C. Pawar, Tae Joon Park*, Jin Geum Kim, Sung-Hoon Ahn, and Caroline Sunyong Lee†**

Department of Materials Engineering, Hanyang University, Ansan 15588, Korea
**Research Institute of Engineering and Technology, Hanyang University, Ansan 15528, Korea*
***Department of Mechanical & Aerospace Engineering, Seoul National University, Seoul 08826, Korea*

(Received May 31, 2016; Revised July 13, 2016; Accepted July 20, 2016)

ABSTRACT

We have successfully fabricated 3D (3-dimensional) nanostructures of TiO_2 coated with a g-C_3N_4 layer via hydrothermal and sintering methods to enhance photoelectrochemical (PEC) performance. Due to the coupling of TiO_2 and g-C_3N_4, the nanostructures exhibited good performance as the higher conduction band of g-C_3N_4, which can be combined with TiO_2. To fabricate 3D nanostructures of g-C_3N_4/TiO_2, TiO_2 was first grown as a double layer structure on FTO (Fluorine-doped tin oxide) substrate at 150°C for 3 h. After this, the g-C_3N_4 layer was coated on the TiO_2 film at 520°C for 4 h. As-prepared samples were varied according to loading of melamine powder, with values of loading of 0.25 g, 0.5 g, 0.75 g, and 1 g. From SEM and TEM analysis, it was possible to clearly observe the 3D sample morphologies. From the PEC measurement, 0.5 g of g-C_3N_4/TiO_2 film was found to exhibit the highest current density of 0.12 mA/cm^2, along with a long-term stability of 5 h. Compared to the pristine TiO_2, and to the 0.25 g, 0.75 g, and 1 g g-C_3N_4/TiO_2 films, the 0.5 g of g-C_3N_4/TiO_2 sample was coated with a thin g-C_3N_4 layer that caused separation of the electrons and the holes; this led to a decreasing recombination. This unique structure can be used in photoelectrochemical applications.

Key words : TiO_2, Graphitic-carbon nitride, Photoelectrochemical, Recombination, Film

1. Introduction

Photoelectrochemical (PEC) electrodes have often been applied to solve energy and environmental issues.[1,2] To produce a PEC electrode, various catalysts can be considered candidates for practical applications. Semiconductor photocatalysts such as TiO_2,[3] Fe_2O_3,[4] WO_3,[5] or ZnO[6] have been studied as efficient materials in this field. Among those materials, TiO_2 is one general material that has been explored as a semiconductor because of its non-toxicity, low cost, easy fabrication, and highly stable chemical and photo-response properties. However, TiO_2 has the drawback of a large band gap (< 3.2 eV), and it absorbs only in the ultraviolet range, which is less than 5% of the solar spectrum. To reduce its band gap energy, TiO_2 has been synthesized with various doping materials or heterogeneous structures including narrow band gap semiconductors such as $ZnFe_2O_4$,[7] CuS,[8] Cu_2O[9] or Bi_2S_3,[10] etc.

Recently, polymeric materials of g-C_3N_4 (graphitic-carbon nitride) are being used as photocatalysts due to their lower band gap energy (> 2.6 eV) and excellent thermal stability at relatively high temperature.[11-14] Particularly, g-C_3N_4 is a stable structure in acid or alkaline based solutions because of the strong covalent bonding of the C-N atoms.[15] However, g-C_3N_4 exhibits fast recombination of electron and hole pairs, which leads to low efficiency in photocatalysis applications. To diminish the defects of g-C_3N_4, there have been several attempts to construct a unique composite. Hence, it has been reported that g-C_3N_4 possesses a higher conduction band than that of TiO_2; this high conduction band is attributed to the couple g-C_3N_4/TiO_2 composite as a stable heterojunction structure.[16-19] In addition to this, to achieve better photocatalytic performance, 1D (1-dimensional) aligned TiO_2 micro/nanorod structures have been explored for rapid electron transfer. However, these 1D structures have poor surface area and efficiency.[20] Hence, to advance the overall performance, 3D (3-dimensional) constructions, such as branched or flower-like shapes, have been under profound consideration in attempts to increase the surface area and the photo-response efficiency. Such 3D structures can be more easily used to facilitate faster movement of electrons than is possible when using 1D structures.

In the present study, using hydrothermal and sintering methods, we explore the fabrication of a g-C_3N_4/TiO_2 film. To control the band gap energy and to diminish the recombination rate as an effective method of separating electron-hole pairs, g-C_3N_4 is coated on double layer TiO_2 structures. Through the mechanism of its 3D nanostructure, g-C_3N_4/TiO_2 can be used to demonstrate its potential. By loading a

†Corresponding author : Caroline Sunyong Lee
E-mail : sunyonglee@hanyang.ac.kr
Tel : +82-31-400-4697 Fax : +82-31-263-4742

thin g-C_3N_4 layer on TiO_2 double layer structures, electron scattering and absorption degree will increase more than is the case for a thick g-C_3N_4 layer because of the transmittance of incident light. Therefore, the use of a g-C_3N_4/TiO_2 film as a 3D nanostructure facilitates electron transport under illumination; it is therefore possible to apply this method to PEC electrode technology.

2. Experimental Procedure

2.1. Preparation of TiO_2 micro/nanorods

TiO_2 micro/nanorods on an FTO substrate were prepared by following a basic hydrothermal process. Before employing the hydrothermal method, FTO substrates were cleaned with ethanol for 30 min. During the cleaning process, TiO_2 solution was prepared. First, deionized water and HCl (Hydrogen chloride, Dae-jung) were mixed at a 1:1 volume ratio. Then, to prevent agglomeration of the Ti precursors, 1 mL of TIPP (Titanium isopropoxide, Sigma-Aldrich) was added drop-wise into the above solution and resulting mixture was stirred vigorously for 30 min. The two cleaned conductive FTO substrates were placed into a Teflon-lined autoclave facing the walls and the autoclave was heated to 150°C; this temperature was maintained for 3 h. After this, the autoclave was cooled to room temperature. Finally, the grown TiO_2 film was rinsed with distilled water and dried at room temperature.

2.2. Sintering process for g-C_3N_4 on TiO_2 film

The coating of the g-C_3N_4 layer was conducted in a crucible with a cover via a sintering process. For the formation of g-C_3N_4, a melamine precursor was obtained from Junsei Chemicals. Using this precursor, sample amounts of melamine if 0.25 g, 0.5 g, 0.75 g, and 1 g were added to the crucible and the prepared TiO_2 film was placed facing down. The crucibles were then heated to 520°C and maintained at that temperature for 4 h to obtain uniform g-C_3N_4 layers; the heating rate was $10^{o}min^{-1}$. Consequently, 0.25 g, 0.5 g, 0.75 g, and 1 g g-C_3N_4/TiO_2 films were successfully obtained.

2.3. Photoelectrochemical performance

The photoelectrochemical (PEC) performance evaluation was conducted to measure the charge carriers under visible illumination (halogen lamp, 100 W). This process used a conventional three-electrode system. Carbon and Ag/AgCl were used for the counter and reference electrodes, respectively. 0.5 M Na_2SO_4 was used as the electrolyte. PEC was conducted with 1 V of applied bias potential versus the Ag/AgCl reference electrode during 4 cycles of on/off under visible light. To determine the long-term stability of the samples, a stability test was carried out for 5 h under the same conditions. LSV (Linear Sweep Voltammetry) analysis was carried out at a 20 mV/s scan rate and -1 to 1 V of potential range.

2.4. Characterization

XRD (X-Ray Diffraction; model D/Max–2500/PC, Rigaku, USA; Cu Kα source) measurement was performed to determine the crystalline structure properties of the TiO_2 phase. The surface morphologies, used to differentiate between TiO_2 and g-C_3N_4, were obtained by SEM (Scanning Electron Microscopy; model S4800, Hitachi, Japan) and TEM (Transmission Electron Microscopy; model JEM 2100F, JEOL, Japan). To observe and calculate the band gap energy of the films, optical absorbance measurement was conducted using UV spectroscopy (UV–Vis; model V650, JASCO, Japan); $BaSO_4$ was used as the reference sample. FT-IR (Fourier-transform infrared spectroscopy; model iS10, Thermo Fisher Scientific, UK) measurement was conducted for observation of the chemical formation of g-C_3N_4. PL (Micro confocal Photoluminescence; model MonoRa750i, DongWoo Optron Co. Ltd, Korea) spectra measurement using a 325 nm excitation light source was conducted to determine the recombination rates of TiO_2 and g-C_3N_4. PEC and LSV analyses were conducted using a potentiostat (model VersaSTAT4, Princeton Applied Research, USA)

3. Results and Discussion

3.1. Structural morphologies

3.1.1 SEM analysis

The surface morphologies of the distinctive g-C_3N_4 and TiO_2 structures were observed using SEM. In Fig. 1(a), it can be seen that TiO_2 micro/nanorods grew as double layer structures; these structures are present in rod shape in the bottom layer and in flower-like shape at the top of the layer. The overall length of the double layer was determined to have an average of 3 μm. Double layer structures are expected to accelerate the movement of electrons and to assist in improving the scattering effect. When the melamine powders were added to the TiO_2 films to form the g-C_3N_4, the morphologies of the resulting mixtures revealed that g-C_3N_4 sheets were coated on the TiO_2 surfaces according to the varying amounts of melamine of 0.25 g, 0.5 g, 0.75 g, and 1 g (Figs. 1(b) ~ (e)). From these microstructures, we can confirm that g-C_3N_4 was added to the TiO_2 rod layer. Only 0.5 g and 1 g of g-C_3N_4/TiO_2 were needed to uniformly cover the g-C_3N_4 on the TiO_2 bottom layer. Moreover, 1 g of the g-C_3N_4/TiO_2 structure was present as a film that was thicker than the other g-C_3N_4/TiO_2 films. According to these results, we can confirm that g-C_3N_4/TiO_2 structures were well-constructed with increasing of the added amounts of g-C_3N_4.

3.1.2 TEM analysis

To accurately determine the size of the g-C_3N_4 layer on TiO_2 structure, TEM analysis was conducted, with results shown in Fig. 2. Here, we tried to compare only TiO_2 rods and a 0.5 g g-C_3N_4/TiO_2 film that we optimized as explained in later sections. As can be seen in Fig. 2(a), the average diameter was observed and found to be ~125 nm, which is in agreement with the SEM results. Importantly, coating thickness can be controlled according to the amount of

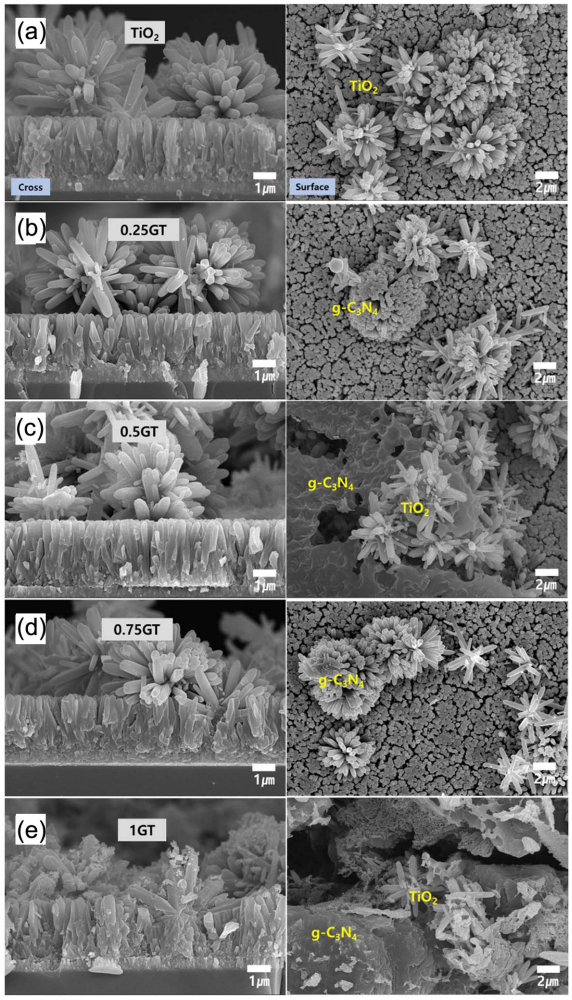

Fig. 1. Surface morphologies of (a) only TiO_2, and (b) 0.25 g , (c) 0.5 g, (d) 0.75 g, and (e) 1 g of g-C_3N_4/TiO_2, observed using SEM.

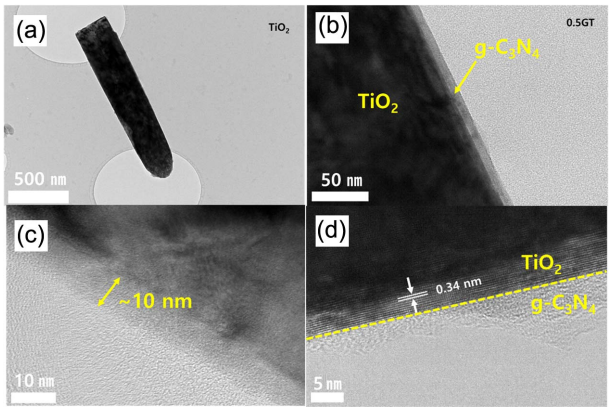

Fig. 2. TEM analysis of (a) only TiO_2, (b), (c) 0.5 g g-C_3N_4/TiO_2, and (d) *d*-spacing of TiO_2.

added melamine. Figs. 2(b) and (c) shows that 0.5 g of g-C_3N_4/TiO_2 leads to an approximately thin ~ 10 nm coating on the TiO_2 rods. Further, according to the SAED (selected area electron diffraction) pattern, TiO_2 and g-C_3N_4 showed

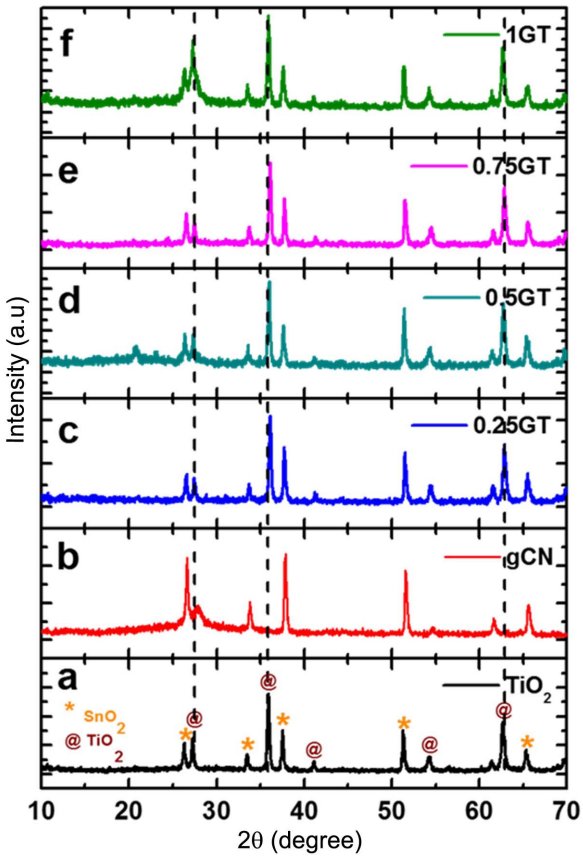

Fig. 3. XRD analysis of (a) TiO_2, (b) g-C_3N_4, and (c) 0.25 g, (d) 0.5 g, (e) 0.75 g, and (f) 1 g of g-C_3N_4/TiO_2.

crystalline and amorphous phases, respectively. The *d*-spacing of the TiO_2 lattice is 0.34 nm (Fig. 2(d)). Therefore, we can confirm the crystallization of TiO_2 from the lattice diffraction pattern and the g-C_3N_4 coating layers on the TiO_2 rods.

3.2. Phase crystallization - X-ray Diffraction

XRD analysis was conducted to examine the TiO_2 crystallinity and the g-C_3N_4 phase structure. As can be seen in Fig. 3, the presence of only TiO_2 peaks indicated the formation of rutile TiO_2 phase, which is exactly correct according to JCPDS card No. 01-078-4190. Additional peaks in the TiO_2 films can be referred to the SnO_2 phase (JCPDS card No. 01-077-0449). Using XRD analysis, the TiO_2 lattice constants were calculated and found to be a = 4.62, c = 2.15 Å and d_{110}=3.26 Å for the tetragonal TiO_2 structure. Pure g-C_3N_4 film showed a peak at around 27°, which means it has an amorphous structure as well, as can be seen in Fig. 3(b). However, it is difficult to differentiate TiO_2 and g-C_3N_4 crystallization from Figs. 3(c) to (f) because the crystal (110) plane of TiO_2 at 27° overlapped exactly with the g-C_3N_4 plane. The amounts of g-C_3N_4 can be correlated with the broadening of the peak at 27 compared to that of the pristine TiO_2 film. Finally, it is proved that TiO_2 is well-crystallized and that the g-C_3N_4 sheet is well formed with TiO_2

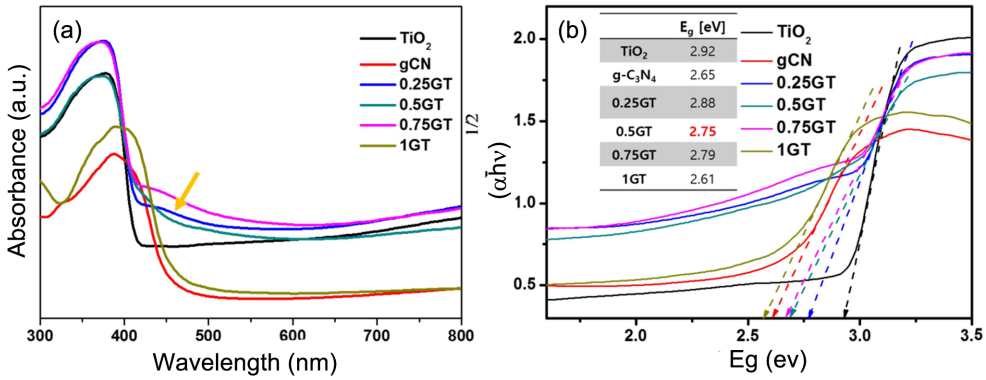

Fig. 4. (a) Optical absorbance and (b) calculation of the band gap energy of TiO_2, g-C_3N_4, and 0.25 g, 0.5 g, 0.75 g, and 1 g of g-C_3N_4/TiO_2.

micro/nanorods.

3.3. Optical absorbance

The degree of absorbance under the visible range can be determined using a UV-Vis spectrophotometer. All films were prepared for measurement of the optical absorbance from 800 to 300 nm. In Fig. 4(a), the absorbance properties of each film can be seen; the TiO_2 film exhibited an absorbance edge at around 420 nm. The film of 0.5 g g-C_3N_4/TiO_2 has an absorbance edge at 440 nm; this means that there is higher absorbance in the visible range. Pure g-C_3N_4 and 1 g g-C_3N_4/TiO_2 film have similar slopes of around 450 nm. Fig. 4(b) presents detailed data on the calculation of the band gap energy of the films. The calculated band gap energies of the samples were 2.92, 2.65, 2.88, 2.75, 2.79, and 2.61 eV for TiO_2, g-C_3N_4, 0.25 g g-C_3N_4/TiO_2, 0.5 g g-C_3N_4/TiO_2, 0.75 g g-C_3N_4/TiO_2, and 1 g g-C_3N_4/TiO_2, respectively. The band gap transitions are obviously revealed to depend on the amount of g-C_3N_4 added. Clearly, it can be seen that band gap energy can be adjusted according to the thickness of the g-C_3N_4 coating. From the band gap transition, because of the high optical absorbance, we can expect an effective generation of charge carriers.

3.4. FT-IR analysis

The existence of g-C_3N_4 was confirmed using the FT-IR spectrum (Fig. 5). The bands of g-C_3N_4 are mainly located from 1650 to 1200 cm^{-1}. The band at 1625 cm^{-1} was assigned to a strong band of the C-N stretching modes. The other bands at 1401, 1317, and 1234 cm^{-1} were related to C-N bonding and represent heterocycle stretching of g-C_3N_4. The band at around 3000 cm^{-1} was found to correspond to H_2O molecules adsorbed on the surface of the g-C_3N_4. The band at 805 cm^{-1} is indicated to the s-triazine ring vibrations of g-C_3N_4. However, 0.25 g g-C_3N_4/TiO_2 and 0.75 g g-C_3N_4/TiO_2 have no distinctive g-C_3N_4 peaks due to their insufficient coating on TiO_2; the low degree of coating can be seen in the SEM images (Figs. 1(b)-(d)). Thus, the existence of g-C_3N_4 was directly confirmed through an observation of the chemical bonding.

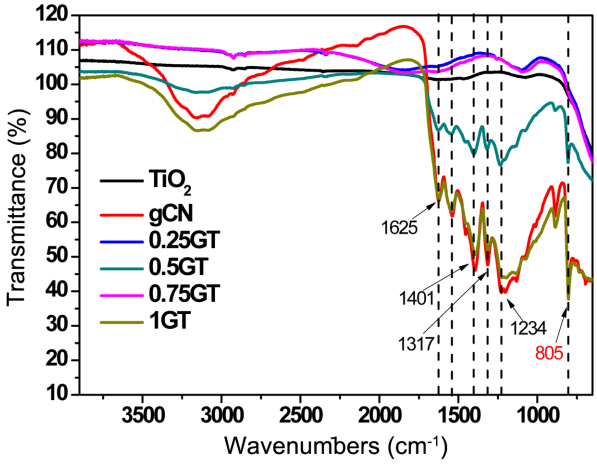

Fig. 5. FT-IR analysis of TiO_2, g-C_3N_4, and 0.25 g, 0.5 g, 0.75 g, and 1 g of g-C_3N_4/TiO_2.

3.5. Photoluminescence

The possibility of charge separation due to g-C_3N_4 addition was observed using photoluminescence (PL) spectra, with results as shown in Fig. 6(a). The strength of PL intensity was found to increase according to the amount of added g-C_3N_4. This means that the recombination rate for this film is faster than that possible with any of the other films. From these results, pure g-C_3N_4 film was found to exhibit the highest intensity of around 500 nm. Then, the loadings of g-C_3N_4 were decreased from 1 g, to 0.75 g, and to 0.5 g of g-C_3N_4/TiO_2. Fig. 6(b) shows that 0.5 g of g-C_3N_4/TiO_2 film has the lowest intensity of PL due to the low recombination of charge carriers. Only the TiO_2 and the 0.25 g g-C_3N_4/TiO_2 films have almost no emission (Fig. 6(c)). The small PL intensity of the TiO_2 film is the result of its relatively porous structure.[21] On the other hand, due to the low level of loading of g-C_3N_4, the 0.25 g g-C_3N_4/TiO_2 film showed trends similar to those of TiO_2. Therefore, we identify that the 0.5 g g-C_3N_4/TiO_2 film was better able to separate electron and hole pairs efficiently and to decrease the recombination rate than the 0.25 g, 0.75 g, and 1 g g-C_3N_4/TiO_2 films.

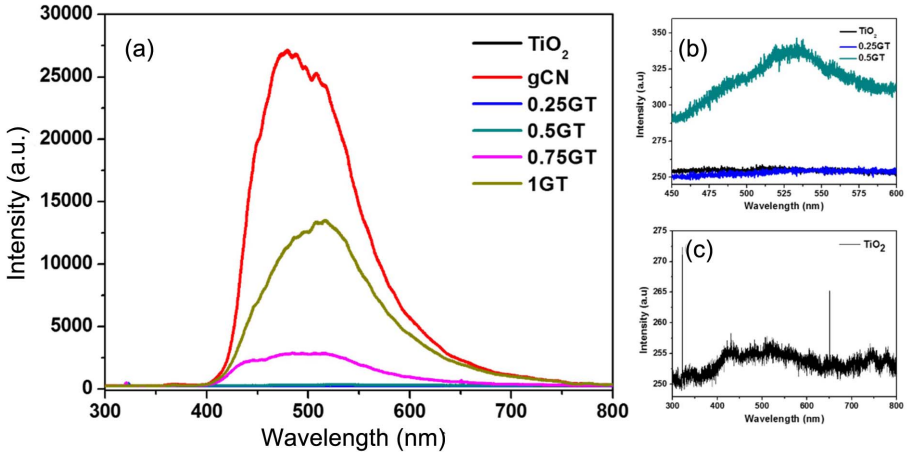

Fig. 6. Photoluminescence of TiO_2, g-C_3N_4, and 0.25 g, 0.5 g, 0.75 g and 1 g of g-C_3N_4/TiO_2.

3.6. Photoelectrochemical analysis

3.6.1 Photocurrent-time (*I-t*) curves

The evaluation of the PEC properties is a significant part of determining the chemical stability. The measurement of the current densities of the as-prepared films was conducted and results are shown in Fig. 7(a). Among the three films, the highest value of current density was obtained for the 0.5 g g-C_3N_4/TiO_2 film at 0.12 mA/cm^2. The second highest current density value was found in the 0.25 g and 0.75 g g-C_3N_4/TiO_2 films, which both had a value of 0.1 mA/cm^2. The TiO_2 film and the 1 g g-C_3N_4/TiO_2 film showed current density values of 0.75 and 0.03 mA/cm^2, respectively. Interestingly, the thicker g-C_3N_4 film, namely the 1 g g-C_3N_4/TiO_2 film, has the lowest current value, lower than even that of the TiO_2 film. This trend could be seen to indicate that the addition of a larger amount g-C_3N_4 does not help the electron transfer efficiency. Moreover, a thicker coating layer might disturb the adsorption of light. Based on the PEC results, the 0.5 g g-C_3N_4/TiO_2 film was used for confirmation of the photoresponse stability, as shown in Fig. 7(b). As well as a higher photoresponse under visible illumination, this film maintained a steady state of its original structure and did not decrease during the 5 h process. There needs to be a proper coating layer on the TiO_2 micro/nanorods; 0.5 g g-C_3N_4/TiO_2 seems to be a suitable material to enhance the PEC properties. Therefore, it is proved that an efficiently applied 0.5 g g-C_3N_4/TiO_2 film can retain stability and can be used for PEC water splitting.

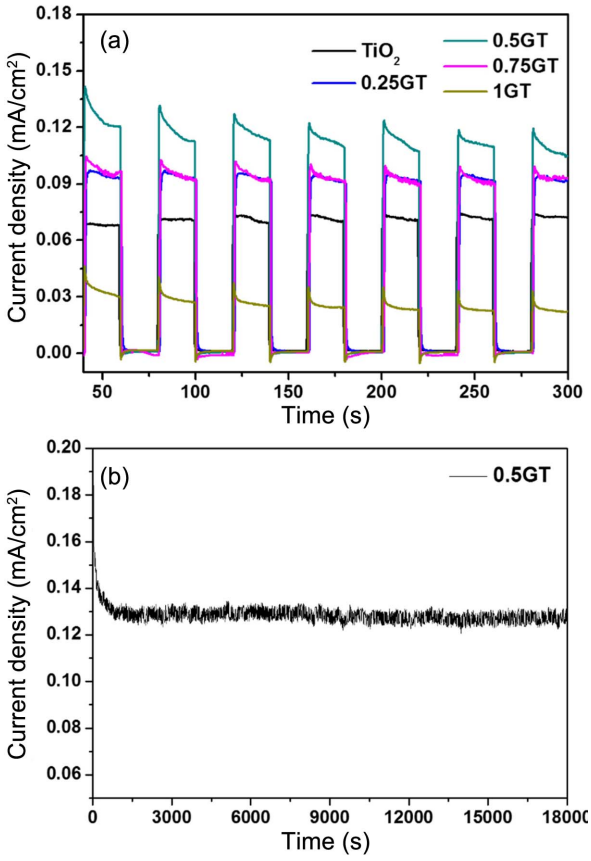

Fig. 7. (a) *I-t* curves of TiO_2, and of 0.25 g, 0.5 g, 0.75 g, and 1 g of g-C_3N_4/TiO_2; (b) Stability test of 0.5 g g-C_3N_4/TiO_2 for 5 h.

3.6.2 LSV

Figure 8 shows linear sweep voltammetry measurement results for TiO_2 only and g-C_3N_4/TiO_2 composite films under a visible lamp. The TiO_2 film shows a 0.8 mA/cm^2 current density, which is the lowest value among the samples. After loading the g-C_3N_4 on TiO_2, a 1 g g-C_3N_4/TiO_2 thick coating film leads to a current density value of 0.12 mA/cm^2. Then, the thinner 0.5 g g-C_3N_4/TiO_2 coating film has a value of 0.21 mA/cm^2 for current density; this is approximately 3 times higher than the value of pristine TiO_2 films (0.8 mA/cm^2). The 0.25 g and 0.75 g g-C_3N_4/TiO_2 films showed lower current density versus potential values than that of the 0.5 g g-C_3N_4/TiO_2 film; however, this film did show a higher current density value than that of the 1 g g-C_3N_4/TiO_2 film. Similar results for PEC and LSV also demonstrated that a thin

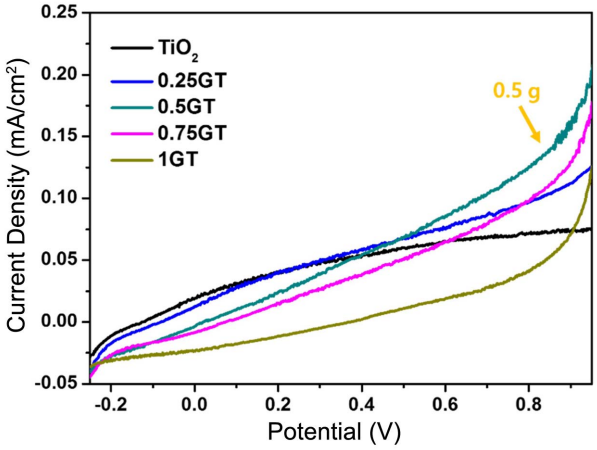

Fig. 8. LSV measurements of TiO_2, and of 0.25 g, 0.5 g, 0.75 g, and 1 g of g-C_3N_4/TiO_2.

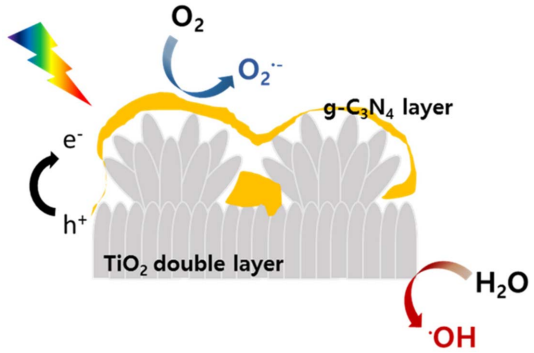

Scheme 1. Schematic mechanism of 3D nanostructure 0.5 g g-C_3N_4/TiO_2 film.

coating of g-C_3N_4 can be used to enhance the current density. Once thick layers are coated on the TiO_2 micro/nanorods, light was not able to reach the TiO_2 surface. The electronic interaction between the TiO_2 and the g-C_3N_4 layer can be used to separate the electrons and the holes efficiently, thus reducing the recombination rate (Scheme 1). Consequently, proper and uniform thickness of the coating layer is necessary for transmission of light to that of surface.

4. Conclusions

We successfully coated a g-C_3N_4 layer on 3D nanostructure grown TiO_2 films via sintering method. Through microstructural and morphological analyses, it was clearly seen that the 3D structure of TiO_2 was grown as a double layer with a flower-like shape on aligned rods. Additionally, a g-C_3N_4 layer was coated onto the TiO_2 double structure. From the FT-IR results, we confirmed the chemical bonding of g-C_3N_4 and the elements Ti, O, N, and C in the g-C_3N_4/TiO_2 film. The g-C_3N_4/TiO_2 films are used to extend the band gap into the visible range. Based on the optical absorbance property and PEC, the recombination rate for electron-hole pairs was found to have decreased. We can definitely prove that proper layer coating is necessary; thus, a 0.5 g g-C_3N_4/TiO_2 film can lead to reduced recombination and enhanced electron transfer properties.

Acknowledgments

This work was supported by the National Research Foundation of Korea (NRF), in a grant funded by the Korean government (MEST) (No.NRF-2015R1A2A1A13027910); by the Industrial Technology Innovation Program of the Korea Evaluation Institute of Industrial Technology (KEIT) granted financial resource from the Ministry of Trade, Industry & Energy, Republic of Korea. (No. 10062510); and by the Human Resources Development program (No.201540 30200680) of the Korea Institute of Energy Technology Evaluation and Planning (KETEP), in a grant funded by the Korean government Ministry of Trade, Industry and Energy.

REFERENCES

1. X. An, T. Li, B. Wen, J. Tang, Z. Hu, L. Liu, J. Qu, C. P. Huang, and H. Liu, "New Insights into Defect-Mediated Heterostructures for Photoelectrochemical Water Splitting," *Adv. Energy Mater.,* **6** [8] 1502268;1-10 (2016).
2. J. Li and N. Wu, "Semiconductor-based Photocatalysts and Photoelectrochemical Cells for Solar Fuel Generation: A Review," *Catal. Sci. Technol.*, **5** [3] 1337-972 (2015).
3. Q. Zhang, J. Lang, J. Su, X. Li, H. Zhai, J. Wang, and J. Yang, "CdS_xSe_{1-x} Nanowhiskers Sensitized Nitrogen-doped TiO_2: 3D-branched Photoelectrode and its Photoelectrochemical Properties," *Chem. Phys.,* **469-470** 79-87 (2016).
4. G. Carraro, C. Maccato, A. Gasparotto, K. Kaunisto, C. Sada, and D. Barreca, "Plasma-Assisted Fabrication of Fe_2O_3-Co_3O_4 Nanomaterials as Anodes for Photoelectrochemical Water Splitting," *Plasma Process Polym.,* **13** [1] 191-200 (2106).
5. Y. Li, X. Wei, X. Yan, J. Cai, A. Zhou, and M. Yang, "Construction of Inorganic-Organic 2D/2D WO_3/g-C_3N_4 Nanosheet Arrays toward Efficient Photoelectrochemical Splitting of Natural Seawater," *Phys. Chem. Chem. Phys.*, **18** [15] 10255-61 (2016).
6. S. Kumar, A. Baruah, S. Tonda, B. Kumar, V. Shanker, and B. Sreedhar, "Cost-Effective and Eco-Friendly Synthesis of Novel and Stable N-doped ZnO/g-C_3N_4 Core–Shell Nanoplates with Excellent Visible-Light Responsive Photocatalysis," *Nanoscale*, **6** [9] 4830-42 (2014).
7. X. Zheng, C. Dinh, F. P. Arquer, B. Zhang, M. Liu, O. Voznyy, Y. Li, G. Knight, S. Hoogland, Z. Lu, X. Du, and E. H. Sargent, "$ZnFe_2O_4$ Leaves Grown on TiO_2 Trees Enhance Photoelectrochemical Water Splitting," *Small*, **12** [23] 3181-88 (2016).
8. G. Fan, H. Zhu, J. Zhang, J. Zhu, and Y. Lin, "Enhanced Photoelectrochemical Immunosensing Platform Based on CdSeTe@CdS:Mn Core–Shell Quantum Dots-Sensitized TiO_2 Amplified by CuS Nanocrystals Conjugated Signal Antibodies," *Anal. Chem.,* **88** [6] 3392-99 (2016).

9. W. Yuan, J. Yuan, J. Xie, and C. M. Li, "Polymer-Mediated Self-Assembly of TiO_2@Cu_2O Core–Shell Nanowire Array for Highly Efficient Photoelectrochemical Water Oxidation," *ACS Appl. Mater. Interfaces*, **8** [9] 6082-92 (2016).
10. L. Zhu and W. Oh, "Novel Bi_2S_3/TiO_2 Heterogeneous Catalyst: Photocatalytic Mechanism for Decolorization of Texbrite Dye and Evaluation of Oxygen Species," *J. Korean Ceram. Soc.*, **53** [1] 56-62 (2016).
11. J. Zhu, P. Xiao, H. Li, and S. A. C. Carabineiro, "Graphitic Carbon Nitride: Synthesis, Properties, and Applications in Catalysis," *ACS Appl. Mater. Interfaces*, **6** [19] 16449-65 (2014).
12. Y. Zhang, Q. Pan, G. Chai, M. Liang, G. Dong, Q. Zhang, and J. Qiu, "Synthesis and Luminescence Mechanism of Multicolor-Emitting g-C_3N_4 Nanopowders by Low Temperature Thermal Condensation of Melamine," *Scientific Reports*, **3** [1943] 1-8 (2013).
13. Y. Zheng, L. Lin, B. Wang, and X. Wang, "Graphitic Carbon Nitride Polymers toward Sustainable Photoredox Catalysis," *Angew. Chem. Int. Ed.,* **54** [44] 12868-84 (2015).
14. H. Dai, X. Gao, E. Liu, Y. Yang, W. Hou, L. Kang, J. Fan, and X. Hu, "Synthesis and Characterization of Graphitic Carbon Nitride Sub-Microspheres Using Microwave Method under Mild Condition," *Diamond Relat. Mater.,* **38** 109-17 (2013).
15. F. Dong, Z. Zhao, T. Xiong, Z. Ni, W. Zhang, Y. Sun, and W. Ho, "In Situ Construction of g-C_3N_4/g-C_3N_4 Metal-Free Heterojunction for Enhanced Visible-Light Photocatalysis," *ACS Appl. Mater. Interfaces,* **5** [21] 11392-401 (2013).
16. Y. Li, R. Wang, H. Li, X. Wei, J. Feng, K. Liu, Y. Dang, and A. Zhou, "Efficient and Stable Photoelectrochemical Seawater Splitting with TiO_2@g-C_3N_4 Nanorod Arrays Decorated by Co-Pi," *J. Phys. Chem. C,* **119** [35] 20283-92 (2015).
17. H. Li, L. Zhou, L. Wang, Y. Liu, J. Lei, and J. Zhang, "In Situ Growth of TiO_2 Nanocrystals on g-C_3N_4 for Enhanced Photocatalytic Performance," *Phys. Chem. Chem. Phys.*, **17** [26] 17406-12 (2015).
18. K. Li, S. Gao, Q. Wang, H. Xu, Z. Wang, B. Huang, Y. Dai, and J. Lu, "In-Situ-Reduced Synthesis of Ti^{3+} Self-Doped TiO_2/g-C_3N_4 Heterojunctions with High Photocatalytic Performance under LED Light Irradiation," *ACS Appl. Mater. Interfaces*, **7** [17] 9023-30 (2015).
19. M. J. Munoz-Batista, A. Kubacka, and M. Fernandez-Garcia, "Effect of g-C_3N_4 Loading on TiO_2-based Photocatalysts: UV and Visible Degradation of Toluene," *Catal. Sci. Technol.*, **4** [7] 2006-15 (2014).
20. F. Su, T. Wang, J. Zhang, P. Zhang, J. Lu, and J. Gong, "Dendritic Au/TiO_2 Nanorod Arrays for Visible-Light Driven Photoelectrochemical Water Splitting," *Nanoscale,* **5** [19] 9001-9 (2013).
21. C. Mercado, Z. Seeley, A. Bandyopadhyay, S. Bose, and J. L. McHale, "Photoluminescence of Dense Nanocrystalline Titanium Dioxide Thin Films: Effect of Doping and Thickness and Relation to Gas Sensing," *ACS Appl. Mater. Interfaces,* **3** [7] 2281-88 (2011).